Fe3+/Fe2+ mycobactin-complex electrochemistry as an approach to determine mycobactin levels in urine.

Journal:	*Electroanalysis*
Manuscript ID:	elan.201400565.R1
Wiley - Manuscript type:	Full Paper
Date Submitted by the Author:	n/a
Complete List of Authors:	Hall, Elizabeth; University of Cambridge, Institute of Biotechnology, Department of Chemical Engineering and Biotechnology McBride, Nicholas; University of Cambridge, Institute of Biotechnology, Department of Chemical Engineering and Biotechnology
Keywords:	mycobacteria, mycobactin, cyclic voltammetry, bovine assay

SCHOLARONE™
Manuscripts

Full Paper   **ELECTROANALYSIS**

Fe³⁺/Fe²⁺ mycobactin-complex electrochemistry as an approach to determine mycobactin levels in urine.

Nicholas S McBride,[a] *Elizabeth A H Hall*[a]*

[a] Institute of Biotechnology, Department of Chemical Engineering and Biotechnology, Tennis Court Road, Cambridge, CB2 1QT, UK

* e-mail: lisa.hall@biotech.cam.ac.uk

Abstract

Mycobacteria acquire iron by producing siderophores called mycobactins, with an extremely high affinity complexation of Fe^{3+}. The iron complex shows distinctive electrochemistry predicting 18 orders of magnitude greater affinity of the mycobactin for Fe^{3+} than Fe^{2+}. A heterogeneous standard rate constant, k_s of the order of 10^{-5} cm s⁻¹ confirms quasi reversible electrochemistry and based on the equilibrium in the presence of excess solution Fe^{3+}/Fe^{2+} the oxidation and reduction peaks for the siderophore complex could be calibrated for ferric mycobactin J (FeMJ). FeMJ spiked urine collected from cows showed a matrix effect on the current peak height. For example, 240±15μM FeMJ was estimated in 600μM spiked urine. However, in the presence of excess solution Fe(acac)₃ the same sample yielded an estimated 580±25μM FeMJ.

Keywords: Mycobacteria, Mycobactin, cyclic voltammetry, bovine assay

1. Introduction

There are more than 150 mycobacteria known, many of which are pathogenic. They generally show a high hydrophobicity with a complex lipid-rich cell wall architecture [1] that is not susceptible to normal antibiotics. The pathogenic species are responsible for a number of diseases, including tuberculosis (TB), Johne's disease, Buruli ulcer and leprosy and may also play a role in chronic bowl diseases, allergies and immunity to other pulmonary infections [2].

In the most highly developed areas of the word the incidence of TB has been reduced, yet the bacterium (*Mycobacterium tuberculosis, Mtb)* continues to infect one-third of the global population with 8.6 million people falling ill and 1.3 million people killed in 2012 [3]. Only a very small percentage of human-mycobacteria interaction turn into full mycobacterial infection, but such progression is much more common in immunocompromised patients. This has led to a great number of clinical TB cases and deaths in populations that have high rates of *Mtb* and HIV coinfection and contributed to a global resurgence of TB [3,4] Areas with particularly high TB burdens include Sub-Saharan Africa and Southeast Asia.

Bovine tuberculosis is caused by the bacterium *Mycobacterium bovis*, which can also infect humans and many other mammals including deer, goats, pigs, cats, dogs and badgers. There are many species of environmental atypical mycobacterioses. *M. avium* subsp. *paratuberculosis* causes Johne's disease in ruminants and has been proposed as a cause of Crohn's disease in humans[5]. Environmental mycobacteria are not obligate pathogens but can be found as saprophytes, commensals, and symbionts. Therefore, the detection and control of *M. tuberculosis* complex organisms and atypical mycobacterioses is important.

In thinking about detection, it is worth considering that iron is a key nutrient, necessary for metabolic function and division. Mycobacteria acquire iron by producing siderophores called mycobactins to harvest iron from their environment. Mycobactins from different mycobacteria exhibit structural variation in their alkyl substitutions and chiral centers, but share the same core salicylate-oxazoline structure, which produces hexadentate iron-chelation chemistry with an extremely high affinity complexation of Fe^{3+} [6,7].

Full Paper

There have been several assays created in order to detect or measure mycobactin in different contexts. The ligand to metal charge transfer, indicative of iron-containing compounds, results in a characteristic absorbance at 450 nm; the desferri- forms lack this 450 nm absorbance peak [8]. Mycobactins also have a major absorbance peak at 220 nm, indicative of amide and aromatic groups [8]. This allows for simple differentiation between the ferric and desferri- forms and has been employed by Gobin and coworkers in combination with reverse-phase high-performance liquid chromatography (HPLC) and mass spectrometry to purify and identify mycobactins [9].

Another common assay utilizes chrome azurol S-shuttle solution (CAS) detect production of any iron-chelating siderophores [10]. When the siderophores chelate iron, removing it from the dye complex, the dye changes from blue to orange. This can be observed as an absorbance extinction at 630 nm. Koedam et al. improved on this method by combining isoelectric focusing with CAS overlay for siderophore detection and differentiation. Another dye-based method for catechol-based siderophores is to use the Arnow assay [11], however this is not typically employed to detect hydroxamate siderophores such as mycobactin. These methods are useful for certain *in vitro* applications, however they lack the versatility required for routine screening.

A bioassay based upon the growth of mycobactin-dependent *M. avium* subsp. *paratuberculosis* was developed by Lambrecht and Collins [12], but this assay failed to detect the presence of mycobactin in infected tissue samples with an estimated sensitivity of 6 nM and a readout time of 21 days. Nevertheless, the features of mycobactins and their Fe^{3+} complexation offer scope for a common assay approach and some potential for distinction according to substitution.

We have sought to investigate the potential for a versatile electrochemical assay for mycobactin that may, in turn, contribute to techniques for an *Mtb* infection assay. This proof-of-concept assay takes advantage of the specific electrochemical properties of mycobactin-chelated iron for detection.

2. Experimental

2.1 Materials

Purified ferric mycobactin J (FeMJ) was purchased from Allied Monitor. Potassium chloride, lithium chloride tris(hydroxymethyl)aminomethane (TRIS), phosphate buffered saline tablet (PBS), hydrochloric acid, sodium hydroxide, chloroform, DMSO, diethyl ether and ethanol were purchased from Sigma-Aldrich. Reagents were used as received without further purification and aqueous solutions were prepared in milli-Q water (resistance 18.2 MΩ/cm).

2.2 Deferration of Mycobactin

Deferration of the FeMJ was accomplished by dissolving 2 mg of mycobactin in 10 mL of chloroform and shaking with 10 mL of 5 M hydrochloric acid. The organic phase was then separated and dried under vacuum to give desferri mycobactin J (DFMJ).

2.3 Electrochemical Experiments

A 3 mm diameter glassy carbon electrode (GCE) was purchased from Bioanalytical Systems, Inc. (BASi) The electrode surface was prepared by polishing successively with 1.0 μm and 0.05 μm alumina powder using MicroCloth polishing cloths (Buehler) affixed to a glass base. Alumina residue was subsequently removed by oxidative cleaning at 0.8 V vs. Ag/AgCl in aqueous 1 M sodium hydroxide and 1 M potassium chloride [13].

Measurements were performed on a Princeton Applied Research 263A potentiostat and a PC running CorrWare software. Unless otherwise noted, all figures and calculations were made using cyclic voltammograms at 0.2 V/s scan rate. For high-speed cyclic voltammetry a Solartron 1286 potentiostat was used in analog mode to drive the potential, while a PicoScope 4224 was used for data acquisition. A custom Matlab program was written to process the high-speed cyclic voltammetry data. The final electrochemical configuration consisted of a platinum wire counter electrode, silver wire pseudo reference electrode, and GCE working electrode in either DMSO containing 0.1 M LiCl or 50% ethanol solution containing 0.1 M KCl supporting electrolyte. Oxygen was removed from the solution by bubbling nitrogen gas for at least 10 min and maintaining a unidirectional gas-flow environment; longer times were required to adequately deoxygenate desferri mycobactin solutions.

2.4 Spiking of Water and Urine Samples

25 mL of either purified, deionized water or female bovine urine was spiked with a stock solution of 5 mM FeMJ in DMSO to give final concentrations of 5 μM FeMJ and 0.1% of the respective solvent. The samples were then subjected to chromatography as outlined below.

Full Paper

2.5 Chromatographic Concentration of Mycobactin

Chromatographic concentration was performed using reverse-phase Waters Sep-Pak tC_{18} cartridges containing 50 mg of sorbent, bead size of 37-55 µm, pore size of 125 Å, and bed volume of 0.13 mL. Elution was performed with 3×0.5 mL of diethyl ether and the eluate was subsequently dried under vacuum. Spectrophotometric analysis was done after dissolving the residue in 0.75 mL methanol or electrochemical analysis was performed after dissolving the residue in 0.1 mL DMSO containing 0.1 M LiCl.

2.6 Bovine Urine Experiments

For the bovine urine experiments, urine was collected from three female cows from the University of Cambridge Department of Veterinary Medicine dairy herd. 25 mL samples were either spiked with 2 µM FeMJ and 0.1% DMSO (final concentration), or left unspiked and frozen at -80°C until chromatography.
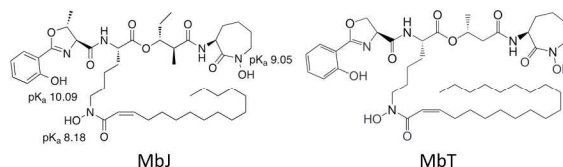
Scheme 1. Structure of *MbJ and MbT* shown with pK_a values for its iron-chelating ligands

3. Results and Discussion

The core structure of mycobactin is shown in scheme 1. Each species of mycobacteria has a defined set of R_{2-6} substituents, while the alkyl chain at R_1 can vary in length (C_{14-20}) and degree of unsaturation. It is common for the alkyl chain to contain a *cis* double bond in the α-β position [14]. Both the cyclic and linear lysine residues are N^6-hydroxylated to form the two hydroxamate metal coordination sites. These, together with an oxazoline-phenolate coordination site, serve to make mycobactin a hexadentate metal coordinator with an extremely high formation constant for complexation for Fe^{3+} (4×10^{26} M^{-1}) [6].
Ferric mycobactin J (FeMJ) was chosen as the model mycobactin for these experiments due to its ready availability in a relatively pure form and similarity to mycobactin T in its core structure and iron-coordination ligands (see scheme 1), as well as its importance in veterinary medicine [5].

3.1 Electrochemistry of mycobactin J

Lipophilic mycobactin J with or without iron is virtually insoluble in aqueous media, so figure 1a shows the current-voltage curves of the siderophore in 1:1 ethanol:water and dimethyl sulfoxide (DMSO). As shown by the method of Harrington et al. [15], the relationship between the reduction potential of the siderophore complex and the reduction of Fe^{3+} in solution is related to the ratio of formation constants according to the Nernst equation:

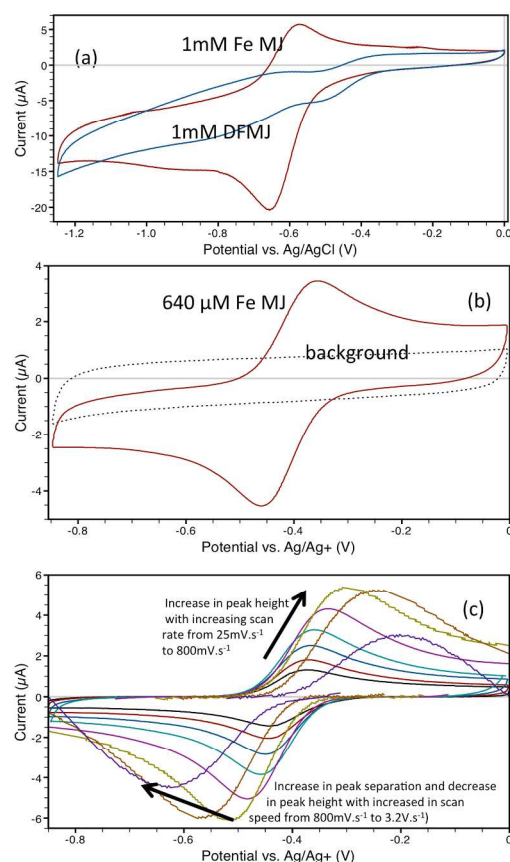$$E^0_{complex} - E_{aq} = -59.16 mV \log\left(\frac{\beta^{III}}{\beta^{II}}\right) \quad \text{Equation 1}$$

Fig. 1. Cyclic voltammograms at 200mV s-1 (a) of FeMJ and DFMJ in 50% ethanol/water with 0.1 M KCl; (b) FeMJ (640µM) in DMSO with 0.1 M LiCl; (c) background-subtracted CVs of FeMJ (640µM) in DMSO with 0.1 M LiCl at different scan rates (25mV/s – 3.2V/s).

where $E^v_{complex}$ is the standard potential for reduction of the complex, E_{aq} is the standard potential for reduction of Fe^{3+} in solution, and β^{III} and β^{II} are the formation

Full Paper

constants for the complex with Fe^{3+} and Fe^{2+} respectively. From the data obtained, this yields a β^{III}/β^{II} ratio of 1.9×10^{18}, signifying 18 orders of magnitude greater affinity of the mycobactin for Fe^{3+} than Fe^{2+}, in agreement with previously published estimations for a water-soluble analogue of mycobactin [15] and in line with its expected high affinity for Fe^{3+} (4×10^{26} M^{-1}) [6]. These affinity kinetics are essential to the iron trafficking mechanism, whereby mycobactin bound ferric ion is transported though the cell wall where iron is removed by its reduction to Fe^{2+} [15,16].
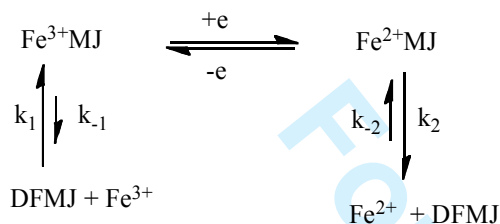
Scheme 2. Redox equilibria for FeMJ with associated $Fe^{2+/3+}$ complexation steps, producing an EC electrochemical mechanism.
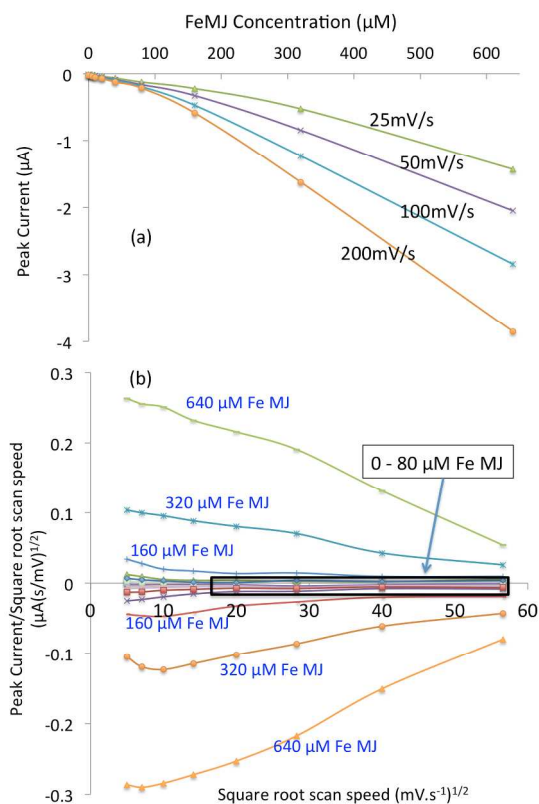

Fig.2 (a) CV reduction peak current versus FeMJ concentration at different scan rates. (b) $i_p/v^{1/2}$ versus $v^{1/2}$ shown for both the reduction and oxidation peaks of FeMJ at concentrations 0, 5, 10, 20, 40, 80,160, 320, 640μM. Data recorded in DMSO, 0.1 M LiCl

Typical cyclic voltammograms (CVs) of FeMJ (Figure 1b and 1c) show a quasi-reversible redox couple, assigned to the mycobactin complexed Fe^{3+}/Fe^{2+} couple, with midpoint potential -0.41 V vs. Ag/Ag^+ (at 25 mV/s, 0.64 mM in DMSO). Calibration curves obtained at different scan speeds (figure 2a, shown for the reduction peak), show that the peak height is proportional to concentration but with deviation from a good linear fit. If this would be a simple electron transfer limited by diffusion, $i_p/v^{1/2}$ should be independent of scan rate (v), as given by a rearrangement of the Randles-Sevcik equation. Diagnostic plots of $i_p/v^{1/2}$ versus $v^{1/2}$ (figure 2b) were independent of scan rate at low concentration and high scan rate (black boxed area in figure 2b), but changed with scan rate at lower scan rates or higher concentrations (>150μM) with a slope increasing with concentration. This points to a coupled electrochemical-chemical pathway. This would be anticipated for a reaction pathway also involving the affinity kinetics between $Fe^{2+/3+}$ and the mycobactin.

The presence of a competing chemical step following reduction is confirmed by $i_{pa}/i_{pc} < 1$ for all scan rates and concentrations. This can be interpreted by dissociation of the Fe^{2+} from the MJ complex upon reduction of Fe^{3+} (k_2 in scheme 2). Consistent with this, i_{pa}/i_{pc} increases (from~0.3 to ~0.8) with scan rate at low FeMJ concentrations. At fast scan rate the electrochemical oxidation of the iron-mycobactin complex competes with the rate of the dissociation, so the oxidation peak is recovered. For a given scan rate, i_{pa}/i_{pc} mostly increases with concentration, suggesting that Fe^{2+} dissociation is influenced by overall siderophore concentration, which could suggest intermolecular exchange of Fe^{2+}.

In order to determine whether the observed redox couple is attributable specifically to the ferric iron chelated by mycobactin, the iron was removed from FeMJ to create DFMJ as described in the materials and methods section. Cyclic voltammograms of DFMJ lacked the peaks characteristic of FeMJ, but upon titration of $Fe(acac)_3$ into the solution, the characteristic peaks returned (figure 3a). Furthermore, upon oversaturation of the 1:1 iron-binding ratio with DFMJ, the redox peaks shifted cathodically, indicating a shift in the equilibrium for the $Fe^{2+/3+}$ MJ complex. Since the $Fe(acac)_3$ redox couple lies at a higher potential (in figure 3a the reduction peak can be seen at -0.28 V with excess $Fe(acac)_3$), then at the potential for FeMJ redox, $Fe(acac)_3$ is reduced producing high Fe^{2+} concentrations near the electrode, driving the k_2/k_{-2} equilibrium away from dissociation. This also results in i_{pa}/i_{pc} approaching unity at low scan rates.

Full Paper

3.2 Kinetics of FeMJ redox

The quasi reversible behaviour of this iron complex is also indicated by the diagnostic plots of E versus log v (figure 3b and c) which yield slopes greater than 30 mV per decade for scan rates greater than 200 mV/s. Interestingly, at low scan rates, peak separation decreases with increase in concentration, lending support to the idea that Fe^{2+} dissociation is reversed in the presence of higher concentrations of FeMJ. Leading on from the theory developed by Nicholson and Shain [17], followed by Klingler and Kochi [18], apparent transfer coefficients β_v and β_w can be estimated, given by:

$$\beta_v = \frac{2.3RT}{2nF}\left[\frac{dE_p}{d\log v}\right]^{-1} \quad \textbf{Equation 2}$$

$$\beta_w = \frac{1.85RT}{nF}\left[E_p - E_{p/2}\right]^{-1} \quad \textbf{Equation 3}$$

Using these solutions, for the data in figure 3, β_v, reduces from ~0.86 at slow scan rate to around 0.36 for scan rates ≥ 0.2 V/s. This agrees well with β_w obtained from equation (3), which tends to ~0.4($\pm$0.1) at high scan rate. According to Klingler and Kochi, good agreement between β_w and β_v (correlated with a reversibility factor < 0.5) allows the electron-transfer rate constant at the CV peak potential $k(E_p)$ to be obtained and thence the heterogeneous standard rate constant, k_s according to:

$$k_s = 2.18\left(\frac{D\beta nF v}{RT}\right)^{1/2}\exp\left[-\frac{\beta^2 nF}{RT}\left(E_{pa}-E_{pc}\right)\right]$$

Assuming a diffusion coefficient, D, of 1.7×10^{-6} cm^2 s^{-1}, this yields $k_s \sim 5\times10^{-3}$ cm s^{-1}. This result is also confirmed by the technique of Gileadi and Eisner [19] which uses the intersect (v_c, figure 3(b)) obtained by extrapolation of the linear fits to the low scan rate data (E$_{pc}$ vs ln$v$) and the high scan rate data. Figure 3(b) shows the peak potential for anodic and cathodic peak as a function of scan speed (x axis: ln$v$) and as a function of FeMJ concentration (shaded areas in figure for anodic and cathodic branch). As can be seen in this figure, at higher FeMJ concentration, the critical scan rate, v_c obtained from this intersect for both anodic and cathodic peaks converge and have a relation with k_s according to [19]:

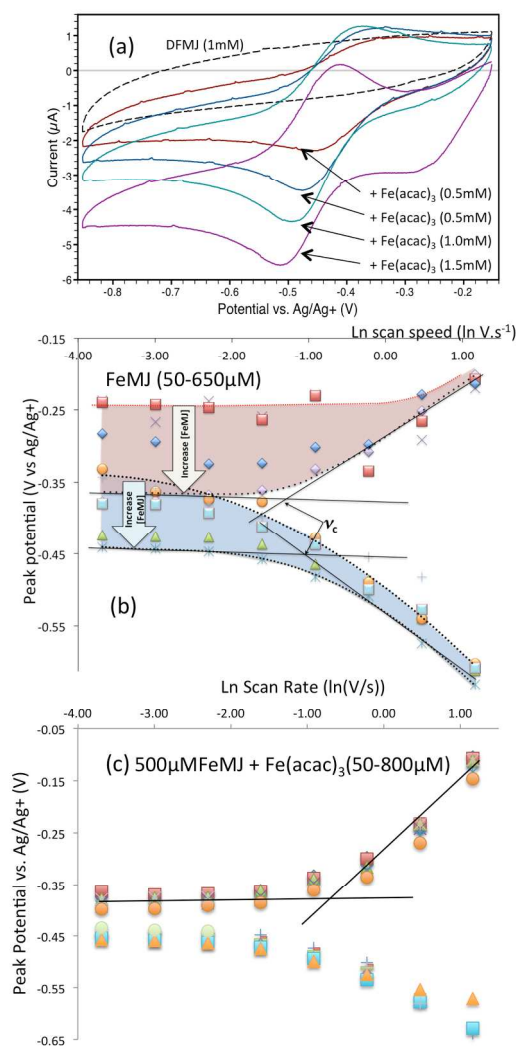$$k_s = -0.48\beta + 0.52 + \ln\left(\frac{D\beta nF v_c}{RT}\right)^{1/2}$$

Fig. 3. (a) CV of referration of DFMJ by titration with Fe(acac)$_3$; 200mV/s in DMSO, 0.1 M LiCl. E$_p$ versus ln v: (b) FeMJ (50-650μM). Bounds of the upper and lower concentration data are indicated by the shaded areas. (c) 0.5 mM FeMJ with addition of 50-800μM(excess) Fe(acac)$_3$. Solid lines in (b) and (c) give linear trend lines for the low and high scan rate data, the intersection gives the critical scan rate (v_c).

which yields $k_s \sim 9\times10^{-3}$ cm s^{-1}.

Based on these findings, quasi reversible electrochemistry is confirmed under these conditions and chemical reversibility is dependent on the concentration ratio of Fe^{3+}, Fe^{2+} and DFMJ and reaches a maximum for DFMJ:Fe^{3+} > 1. So, the CV will be dependent on [Fe^{3+}] according to the equilibrium described by k_1/k_{-1} and k_2/k_{-2} (scheme 1) and taking into account that Fe^{2+} will be

Full Paper

produced at the electrode at the FeMJ redox potential in the presence of solution Fe^{3+}.

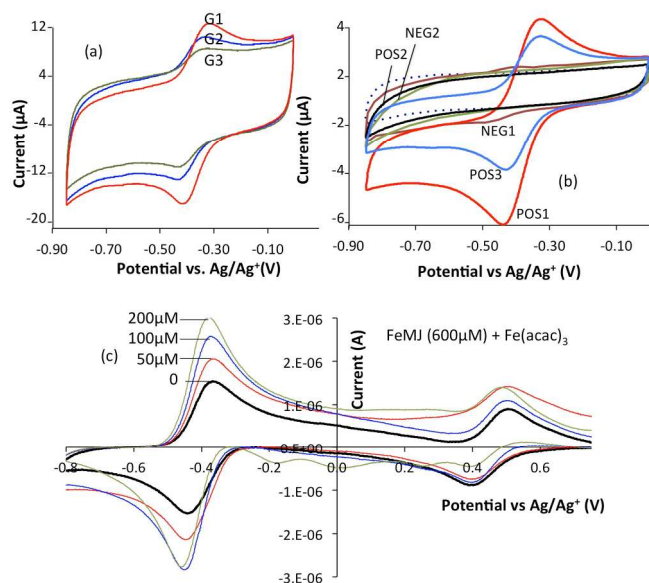Fig. 4 CV's of bovine urine after Sep-Pak tC_{18} elution from (a) cows (G1, G2, G3) spiked with 600μM FeMJ. (b) cow C3: NEG1 unfiltered; NEG2 0.22μm filtered; POS1 unfiltered spiked with 500μMFeMJ; POS2 spiked with 500μMFeMJ and then filtered; POS3 filtered and then spiked with 500μMFeMJ; background is dotted line. (c) Background subtracted CVs with 600μM FeMJ added together with 0 - 200μM $Fe(acac)_3$; 200mV/s. in DMSO with 0.1 M LiCl

3.3 Bovine urine-sample electrochemistry

Data from spiked filtered cow's urine samples (figure 4) show a well-resolved FeMJ redox peak. Nevertheless, despite the same concentration of FeMJ, the peak-height for each sample is different, as can be seen in figure 4a. Based on the calibration in figure 2a, recovery rates for spiked urine were typically found in the range 40-100%, suggesting a matrix effect, influencing the equilibria in scheme 2.

The ferric mycobactins can also be detected by their characteristic absorbance around 450 nm, indicative of iron-containing compounds [9]. Samples from three exemplar cows with and without the same concentration of added FeMJ also produce different increases in absorbance as seen in figure 5b.

If the sample matrix influences the FeMJ complex stability (scheme 2), this is not altogether surprising since the absorbance will be influenced by availability of free $Fe^{2+/3+}$ in the sample. Figure 5a shows the development

of the 452nm peak for DFMJ in the presence of ferric chloride, which highlights the 1:1 stoichiometry between Fe and MJ, as predicted also from the electrochemistry and demonstrates how the absorbance measured will depend on the free Fe^{3+}. Furthermore, mycobactins have a strong amphipathic character, whose solubility and dispersion in urine will depend on other content. This will also influence the apparent concentration measured and the ferric mycobactin complex equilibrium. Conventionally, mycobactins have been thought to be associated with the cell wall and membrane of the mycobacteria. They have low solubility in water (5-10 μg/mL) [14], and upon binding iron, the hydrophilic peptidic head is turned inward to coordinate the central iron atom [20] creating a more compact, less flexible conformation, but with the external surface dominated by the lipophilic character of the alkyl chain. Research on related siderophores, the marinobactins, has shown that the desferri form of the siderophore is capable of forming micelles [21]. The marinobactins have a more overall hydrophilic character than mycobactins, but share the attribute of a single C_{12-16} alkyl chain, making them highly amphipathic. This gives rise to a conical molecular shape in which the hydrophilic iron-coordinating ligands are spread out on the surface of the micelle. Upon binding iron, marinobactins undergo a phase change to form bilayered vesicles [21].

T he issue is especially highlighted for urine sample C3. An unfiltered sample of C3 shows considerable background absorbance in the range from 350-500nm which could be taken for mycobactin infection. Although TB reactors had been seen in the heard previously, the herd had been tested clear before the samples were taken. Notwithstanding this, the full environmental and immunological scope of commonly found mycobacteria remains largely unexplored, and many types of mycobacteria have been isolated from cultivated land in England, including the known mycobactin producers *M. aurum, M. fortuitum, M. intercellulare, M. kansasii, M. marinum, M. phlei, M. scrofulaceum, M. smegmatis, thermoresistibile*, and others [22]. Current tests for the pathogenic strains of *M. bovis* are not targeted to these other environmental organisms, though false positive tests for paratuberculosis in the faeces of ruminants have been known to occur experimentally [23]. Furthermore, testing for Johne's disease is not routinely carried out, given the cumbersome nature of current methods, which rely on culturing the slow-growing organism in the presence of exogenous mycobactin. However, a case of Johne's disease was detected in the herd a few months after these samples were taken.
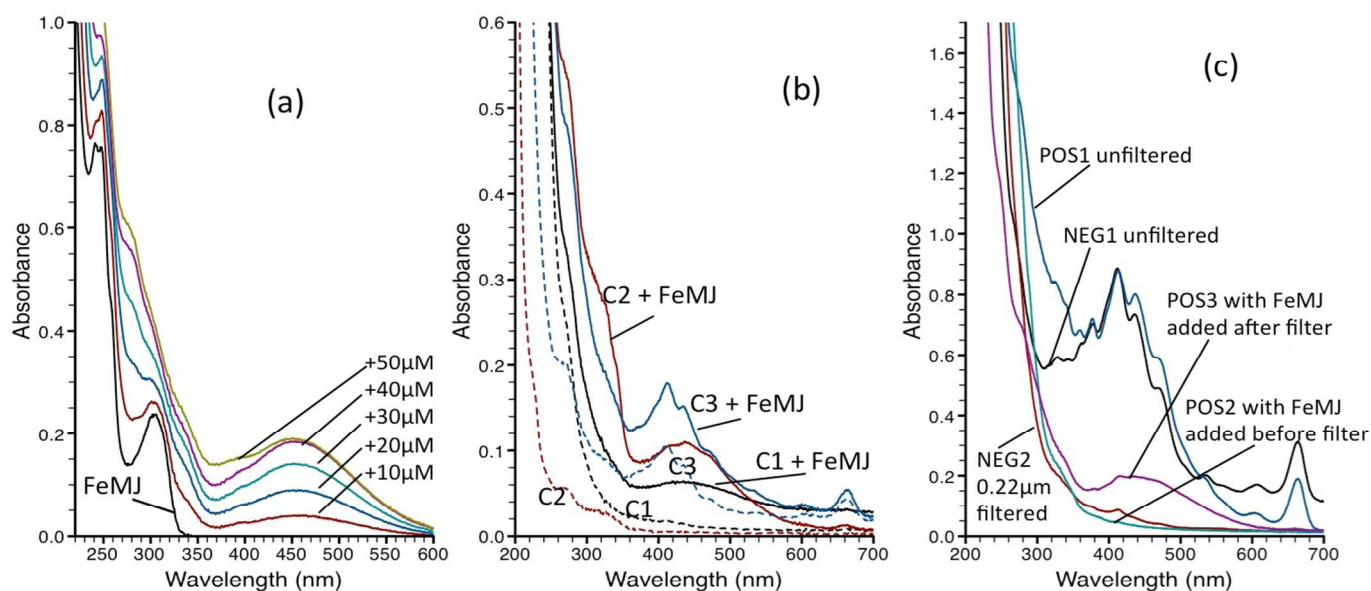
Fig 5. UV-Vis absorption spectra measured in methanol for (a) titration for ferric chloride (0 – 50 μM) into deferrated MJ (DFMJ). (b) samples of bovine urine Sep-Pak tC_{18} eluates in 0.75 mL methanol; C1-C3 refer to samples take from three individual cows with and without the addition of 2 μM FeMJ. (c) Analysis of Sep-Pak tC_{18} eluates from the bovine urine samples from a single urine pool and treated as described in materials and methods.

Passing the C3 sample through a 0.22μm filter (which also removes any bacterial infection) reduced the absorbance in this region (compare curves NEG1 and NEG2 in figure 5c), but this filter also removes the FeMJ (compare C3 with 500μM added FeMJ before (POS1) and after filtration (POS2), figure 5c). Nevertheless, the same concentration of FeMJ added after filtration (POS3) gives a clear absorbance around 450nm, but this is still prone to background sample effects on the measurement. Looking at the electrochemistry of this sample (figure 4b) also shows conflicting estimates of FeMJ and interestingly, there is a small peak in the NEG1 sample, which has no added FeMJ. This agrees with the absorbance date in figure 5b and c, which may be indicative of mycobactin.

In view of these potential matrix effects and presuming that the sample matrix disturbs the equilibria in scheme 2, a strategy for signal 'normalisation' is proposed. The effect on the peak currents in the CV (figure 4c) can be seen for a sample spiked with 600μM FeMJ, with added $Fe(acac)_3$. This demonstrates the shift in the equilibrium (scheme 2) as a result of free $Fe^{2+/3+}$. Taking this initiative, added $Fe(acac)_3$ can be seen to increase the peak-heights for the spiked urine samples recorded in figure 4a (figure 6). From these results, the predicted concentration of FeMJ measure from the shaded area in figure 6, would be 580±25μM whereas from the peak-heights taken from figure 4a only 240±15μM FeMJ was estimated in the assay. This method, which takes into

account the kinetics of the FeMJ complex formation, yields estimates >90% of the spiked FeMJ concentration, compared with the outcome without added $Fe(acac)_3$ of 40±10%.
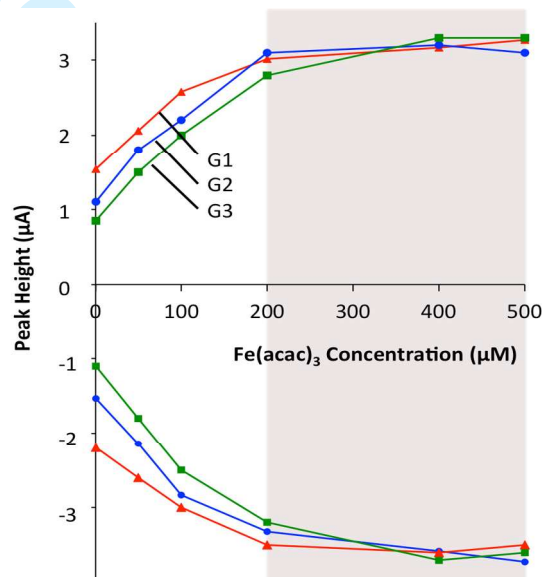

Fig.6 Peak height measured from the oxidation and reduction peaks in the cyclic voltammogram (200mV/s. in DMSO with 0.1 M LiCl) for urine samples G1, G2 and G3 spiked with 600μM FeMJ. CV's recorded with and without added $Fe(acac)_3$ (x axis).

Full Paper

4. Conclusions

This assay, based on iron-chelated mycobactin, exploits the high affinity of mycobactins for Fe^{3+}. This enables the $Fe^{3+/2+}$ electrochemistry to be used as an indicator of the presence of mycobactin. The redox potential is dependent on the mycobactin and pFe value for the ligand [15]. This is well separated from the uncomplexed $Fe^{3+/2+}$ electrochemistry making the identification possible. Nevertheless, the difference in affinity of mycobactin between the Fe^{3+} and Fe^{2+} creates an EC mechanism, which is influenced by the $Fe^{3+/2+}$ concentrations in solution and disturbed by the sample matrix. This has the capacity to affect the peak currents for the siderophore complexed $Fe^{3+/2+}$, as a result of the equilibrium position in scheme 2. Nevertheless, addition of an excess of $Fe(acac)_3$ to the sample pushes that equilibrium towards the siderophore complex, allowing a more reliable and quantitative assay of mycobactin J to be demonstrated, even in different urine samples with a significant matrix effect.

As mentioned earlier, analysis for many mycobactins is not straightforward, so not undertaken routinely. A simple electrochemical assay for mycobactin could serve as a diagnostic. Furthermore, aside from the pathogenic disease role, some mycobactins have also been investigated for a variety of therapeutic applications spanning from chelation therapy agents and anti-cancer agents to antimicrobials. Chelation therapy is used to treat conditions that arise due to undesirable or excess quantities of metal within the body. These can include therapies for heavy metal toxicity [24] and the removal of internal radioactive contamination. Treatment for the removal of excess iron is the most common type of chelation therapy and is routinely carried out for the treatment of acute iron poisoning and chronic iron overload, such as hemochromatosis [25]. Deferoxamine, deferasirox, and deferiprone are all pharmaceutical agents in use for iron-specific chelation therapy. The first of these agents, deferoxamine, was originally discovered as the siderophore of *Streptomyces pilosus*. Because of the disruption that aggressive iron chelation could have on iron homeostasis, it is desirable to closely monitor concentrations of the therapeutic mycobactin and its chelated iron content upon excretion. Thus, the electrochemical assay investigated in the research reported here could have capability to be developed into a simple urine test to monitor dosage. Pharmaceutical companies have been increasingly turning to companion diagnostics as a means to improve safety and efficacy of new prospective pharmaceuticals [26].

6. References

[1] D. Alsteens, C. Verbelen, E. Dague, D. Raze, A. Baulard, Y. Dufrêne, *Pflügers Archiv European Journal of Physiology* **2007**, 456(1), 117-125.

[2] T. P. Primm, C. A. Lucero and J. O. Falkinham III, *Clin. Microbiol. Rev.* **2004,** *17*, 98-106

[3] World Health Organization, Global tuberculosis report 2013, *World Health Organization* **2013**.

[4] C. E. Barry, 3rd, H. I. Boshoff, V. Dartois, T. Dick, S. Ehrt, J. Flynn, D. Schnappinger, R. J. Wilkinson, D. Young, *Nat Rev Microbiol* **2009,** *7*, 845-855.

[5] J. E. Harris and A. M. Lammerding. *J. Food Prot.* **2001,** *64*, 2103-2110.

[6] J. J. De Voss, K. Rutter, B. G. Schroeder, & C. E. Barry, 3rd. *J Bacteriol* **1999,** *181*, 4443-4451.

[7] Kastrinsky, D. B., McBride, N. S., Backus, K. M., LeBlanc, J. J., Barry, C. E., 3rd, *Comprehensive Natural Products II: Chemistry and Biology.* (Eds L. Mander, H.-W Liu) Elsevier: **2010**, Vol. 1, pp 65-145.

[8] S. J. Lane, P. S. Marshall, R. J. Upton, & C. Ratledge, *BioMetals* **1998,** *11*, 13-20.

[9] J. Gobin, & M. Horwitz, *J. Exp. Med.* **1996,** *183*, 1527-1532.

[10] B. Schwyn, & J. B. Neilands, *Anal Biochem* **1987,** *160*, 47-56.

[11] L. E. Arnow. *J. Biol. Chem.* **1937**, *118*, 531-537.

[12] R. S. Lambrecht, & M. T. Collins. *Microbial Pathogenesis* **1993,** *14*, 229-238.

[13] G. K. Kiema, M. Aktay, M. T. McDermott, *Journal of Electroanalytical Chemistry* **2003**, 540, 7-15.

[14] G. A. Snow, *Bacteriol Rev* **1970,** *34*, 99-125.

[15] J. M. Harrington, H. Park, Y. Ying, J. Hong, & A. L. Crumbliss, *Metallomics* **2011**, *3*, 464-471.

[16] G. Rodriguez, R. Gardner, N. Kaur, & O. Phanstiel, *BioMetals* **2008,** *21*, 93-103.

[17] R. S. Nicholson, & I. Shain. *Analytical Chemistry* **1964,** *36*, 706-723.

[18] R. J. Klingler, & J. K. Kochi, *The Journal of Physical Chemistry* **1981**, *85*, 1731-1741.

[19] E. Gileadi and U. Eisner, *J. Electroanal. Chem*. 1970, *28*, 81.

Full Paper

[20] E. Hough, & D. Rogers, *Biochemical and Biophysical Research Communications* **1974,** *57*, 73-77.

[21] J. S. Martinez, G. P. Zhang, P. D. Holt, H.-T. Jung, C. J. Carrano, M. G. Haygood, A. Butler, *Science* **2000,** *287*, 1245-1247.

[22] H. D. Donoghue, E. Overend, and J. L. Standford, *Journal of Applied Microbiology* **1997**, *82(1)*, 57-67.

[23] D. V. Cousins, R. Whittington, I. Marsh, A. Masters, R. J. Evans, and P. Kluver, *Molecular and Cellular Probes* **1999,** *13(6),* 431-442.

[24] H. V. Aposhian. *Annu Rev Pharmacol, Toxicol* **1983**, *23*, 193-215.

[25] D. S. Kalinowski, & D. R. Richardson, *Pharmacol Rev* **2005,** *57*, 547-583

[26] A. C. Wolff, M. E. H. Hammond, J. N. Schwartz, K. L. Hagerty, D. C. Allred, R. J. Cote, M. Dowsett, P. L. Fitzgibbons, W. M. Hanna, A.Langer, L. M. McShane, S.Paik, M. D. Pegram, E. A. Perez, M. F. Press, A. Rhodes, C. Sturgeon, S. E. Taube, R. Tubbs, G. H. Vance, M. T. van de Vijver, M. Wheeler, D. F. Hayes, *J Clin Oncol* **2007**, *25 (1)*, 118-45.